Article

TRANSPARENT PROCESS OPEN ACCESS

THE EMBO JOURNAL

Analysis of acetylation stoichiometry suggests that SIRT3 repairs nonenzymatic acetylation lesions

Brian T Weinert[1,*], Tarek Moustafa[2], Vytautas Iesmantavicius[1], Rudolf Zechner[3] & Chunaram Choudhary[1,**]

Abstract

Acetylation is frequently detected on mitochondrial enzymes, and the sirtuin deacetylase SIRT3 is thought to regulate metabolism by deacetylating mitochondrial proteins. However, the stoichiometry of acetylation has not been studied and is important for understanding whether SIRT3 regulates or suppresses acetylation. Using quantitative mass spectrometry, we measured acetylation stoichiometry in mouse liver tissue and found that SIRT3 suppressed acetylation to a very low stoichiometry at its target sites. By examining acetylation changes in the liver, heart, brain, and brown adipose tissue of fasted mice, we found that SIRT3-targeted sites were mostly unaffected by fasting, a dietary manipulation that is thought to regulate metabolism through SIRT3-dependent deacetylation. Globally increased mitochondrial acetylation in fasted liver tissue, higher stoichiometry at mitochondrial acetylation sites, and greater sensitivity of SIRT3-targeted sites to chemical acetylation *in vitro* and fasting-induced acetylation *in vivo*, suggest a nonenzymatic mechanism of acetylation. Our data indicate that most mitochondrial acetylation occurs as a low-level nonenzymatic protein lesion and that SIRT3 functions as a protein repair factor that removes acetylation lesions from lysine residues.

Keywords acetylation; mass spectrometry; proteomics; SIRT3; stoichiometry
Subject Categories Metabolism; Post-translational Modifications, Proteolysis & Proteomics
DOI 10.15252/embj.201591271 | Received 12 February 2015 | Revised 14 August 2015 | Accepted 20 August 2015 | Published online 10 September 2015
The EMBO Journal (2015) 34: 2620–2632

See also: **DB Lombard *et al*** (November 2015)

Introduction

Lysine acetylation is a reversible protein posttranslational modification (PTM) that regulates protein function. The role of acetylation in regulating chromatin structure and gene transcription is well studied with both lysine acetyltransferases and deacetylases taking part (Shahbazian & Grunstein, 2007). Mass spectrometry (MS), combined with acetylated peptide enrichment, has enabled the identification of thousands of acetylation sites on diverse proteins (Kim *et al*, 2006; Choudhary *et al*, 2009; Lundby *et al*, 2012), implicating acetylation in regulating various cellular processes. Metabolic proteins, particularly in mitochondria, were found to be frequently acetylated, and a multitude of studies have investigated the role of acetylation in regulating metabolism (Wang *et al*, 2010; Zhao *et al*, 2010; Newman *et al*, 2012). While thousands of acetylation sites have been identified on mitochondrial proteins, few acetyltransferases have been implicated in their regulation (Scott *et al*, 2012; Fan *et al*, 2014), and recent studies suggest most mitochondrial acetylation occurs nonenzymatically through exposure to acetyl-CoA (Wagner & Payne, 2013; Pougovkina *et al*, 2014; Weinert *et al*, 2014).

The mitochondrial sirtuin deacetylase SIRT3 regulates acetylation at hundreds of sites (Sol *et al*, 2012; Hebert *et al*, 2013; Rardin *et al*, 2013b), and SIRT3 levels are increased by dietary manipulations such as calorie restriction and fasting (Shi *et al*, 2005; Palacios *et al*, 2009; Hirschey *et al*, 2010; Tao *et al*, 2010; Newman *et al*, 2012). Several studies have suggested that calorie restriction regulates metabolism through SIRT3-mediated deacetylation of mitochondrial enzymes (Hirschey *et al*, 2010; Qiu *et al*, 2010; Shimazu *et al*, 2010; Someya *et al*, 2010; Hallows *et al*, 2011; Hebert *et al*, 2013). However, it is unclear whether SIRT3 is activated to regulate protein function in response to metabolic changes or whether SIRT3 constitutively deacetylates proteins to preserve their normal function. Notably, acetylation typically inhibits the catalytic activity of mitochondrial enzymes and deacetylation by SIRT3 rescues their activity (Lin *et al*, 2012; Ghanta *et al*, 2013). A recent review suggested that nonenzymatic acetylation may represent a type of "carbon stress" which SIRT3 counteracts to ensure metabolic fidelity in mitochondria (Wagner & Hirschey, 2014). If this were the case, we would expect that SIRT3 suppresses acetylation to very low stoichiometry under both basal conditions and the conditions that cause increased acetylation of mitochondrial proteins, such as calorie restriction and fasting.

In this study, we used quantitative MS to estimate acetylation stoichiometry in mouse liver tissue with a particular focus on SIRT3-targeted sites. We used a knockout mouse model for adipose triglyceride lipase (ATGL) to study the dependence of mitochondrial

1 The NNF Center for Protein Research, Faculty of Health Sciences, University of Copenhagen, Copenhagen, Denmark
2 Division of Gastroenterology and Hepatology, Medical University Graz, Graz, Austria
3 Institute of Molecular Biosciences, University of Graz, Graz, Austria
*Corresponding author. Tel: +45 40607184; E-mail: briantate.weinert@cpr.ku.dk
**Corresponding author. Tel: +45 35325020; E-mail: chuna.choudhary@cpr.ku.dk

acetylation dynamics on fatty acid oxidation in the liver, heart, brain, and brown adipose tissues of fed and fasted mice. Our data indicate that most acetylation occurs at very low stoichiometry (< 0.1%), that SIRT3 suppresses acetylation to background levels, and that SIRT3-targeted sites are only modestly affected by dietary manipulations such as fasting and calorie restriction, suggesting that a major role of SIRT3 is to remove acetylation lesions on mitochondrial proteins.

Results

Method used to estimate acetylation stoichiometry

We previously showed that partial chemical acetylation could be used to estimate acetylation stoichiometry (Weinert *et al*, 2014). In this study, we partially acetylated denatured proteins, measured the relative increase in acetylated peptide abundance and the median decrease in all corresponding unmodified peptides (CPs) (Fig 1A). The median degree (%) of partial chemical acetylation is equal to 1 minus the median CP ratio; thus, for a fixed degree of chemical acetylation (5%), the CP ratios will be constant (0.95) while the acetylated peptide ratios will depend on the initial stoichiometry of acetylation (Fig 1B). Acetylation stoichiometry was calculated based on the relative increase in acetylation (acetylated peptide ratio) and the median decrease in CPs (CP ratio) using a previously described formula (Olsen *et al*, 2010) (Fig 1C).

Quantification of acetylated peptide and corresponding peptide ratios

We partially acetylated liver proteins *in vitro* under denaturing conditions using three concentrations of acetyl phosphate (AcP). The relative increase in acetylation at individual sites (acetylated peptide ratios) was quantified by MS using two different methods, stable isotope labeling by amino acids (SILAC) (Ong *et al*, 2002) and tandem mass tags (TMT) (Thompson *et al*, 2003) (Datasets EV1 and EV2). AcP caused increased acetylation relative to untreated control samples in a concentration-dependent manner at nearly all quantified acetylation sites (Fig 1D).

Because of the low level of partial chemical acetylation, we were unable to accurately measure the reduction in CP abundance for individual peptides, as this reduction was less than the resolution of SILAC or TMT quantification in our experiments. In order to overcome this limitation, we devised a method to examine decreased CP abundance at a population level using an internally controlled comparison based on thousands of peptide measurements (see Materials and Methods). We validated this approach by showing that median CP ratios were reduced by chemical acetylation in a concentration- and pH-dependent manner and that the degree of acetylation predicted from the median CP ratios was correlated with the number of acetylation sites detected in these samples (Appendix Fig S1). Partial chemical acetylation caused a significant reduction in median CP ratios as detected by both quantitative methods (Fig 1E). The median CP ratio at 100 mM AcP was 0.96 (TMT quantification) or 0.95 (SILAC quantification), indicating 4% or 5% chemical acetylation, respectively. Since TMT quantification can be affected by parent ion interference, which buffers ratio changes toward the median (Ting *et al*, 2011), we used the median CP ratio based on SILAC quantification for calculating acetylation stoichiometry.

We calculated acetylation stoichiometry from samples treated with 100 mM AcP using the equation shown in Fig 1C, the acetylated peptide ratios for individual sites (Datasets EV1 and EV2), and a median CP ratio of 0.95. SIRT3-targeted acetylation sites (defined as having > 2-fold (S3 > 2), > 4-fold (S3 > 4), or > 8-fold (S3 > 8) increased acetylation in liver tissue from SIRT3 knockout (KO) mice (Hebert *et al*, 2013)) had lower median CP ratios (Fig 1E), suggesting a slightly greater degree of chemical acetylation at these sites. Therefore, to more accurately estimate stoichiometry at SIRT3-targeted sites, we used the median CP ratios shown in Fig 1E to calculate stoichiometry at these sites (0.94 for S3 > 2, 0.93 for S3 > 4, and 0.92 for S3 > 8). We consider these stoichiometry calculations to be estimates, since the CP ratios for individual sites were not determined and the degree of chemical acetylation at individual sites may be variable. In addition, we cannot account for additional modifications at these positions, the presence of which would cause us to overestimate acetylation stoichiometry.

Validating estimated acetylation stoichiometry

In order to directly validate our stoichiometry estimates, we devised a spike-in absolute quantification (AQUA) approach using heavy-isotope-labeled peptide standards (AQUA peptides) (Gerber *et al*, 2003). We spiked in acetylated AQUA peptides at 0.01%, 0.1%, and 1% stoichiometry and used affinity enrichment to enable the detection of both native and AQUA peptides (Fig 2A and B, and Dataset EV3). Acetylation stoichiometry determined by AQUA was significantly correlated with our stoichiometry estimates based on partial chemical acetylation (Fig 2C). To further validate our stoichiometry estimates at a larger number of sites, we used comprehensive (100%) chemical acetylation to essentially generate hundreds of acetylated AQUA peptides. Comprehensively acetylated proteins were mixed with unlabeled liver proteins to 0.01%, 0.1%, and 1% stoichiometry, prior to affinity enrichment of acetylated peptides and SILAC quantification by MS (Dataset EV4, Materials and Methods). Stoichiometry estimates based on 100% chemical acetylation were highly significantly correlated with our estimates based on 5% chemical acetylation, were similar in magnitude, and showed low variability (Fig 2D). Together, these data provide confidence in the accuracy of our stoichiometry estimates based on partial chemical acetylation.

Stoichiometry estimates based on SILAC and TMT quantification were poorly, yet significantly correlated (Appendix Fig S2A). Similarly, estimates based on TMT quantification were poorly correlated with estimates based on 100% chemical acetylation (Appendix Fig S2B). For this reason, all subsequent analyses of acetylation stoichiometry are based on SILAC quantification (unless otherwise noted). Although less accurate for individual sites, the estimates based on TMT quantification were comparable to SILAC for different classes of acetylation sites (Appendix Fig S2C) and are presented in Dataset EV2 as an additional resource.

Acetylation levels in the four-month-old mouse liver tissue used to estimate stoichiometry in this study were comparable to acetylation levels in liver tissues from one-, eight-, and sixteen-month-old animals (Fig 2E). Acetylation levels were also similar in SILAC liver tissue, liver tissue from an independent source (wild-type (WT) fed

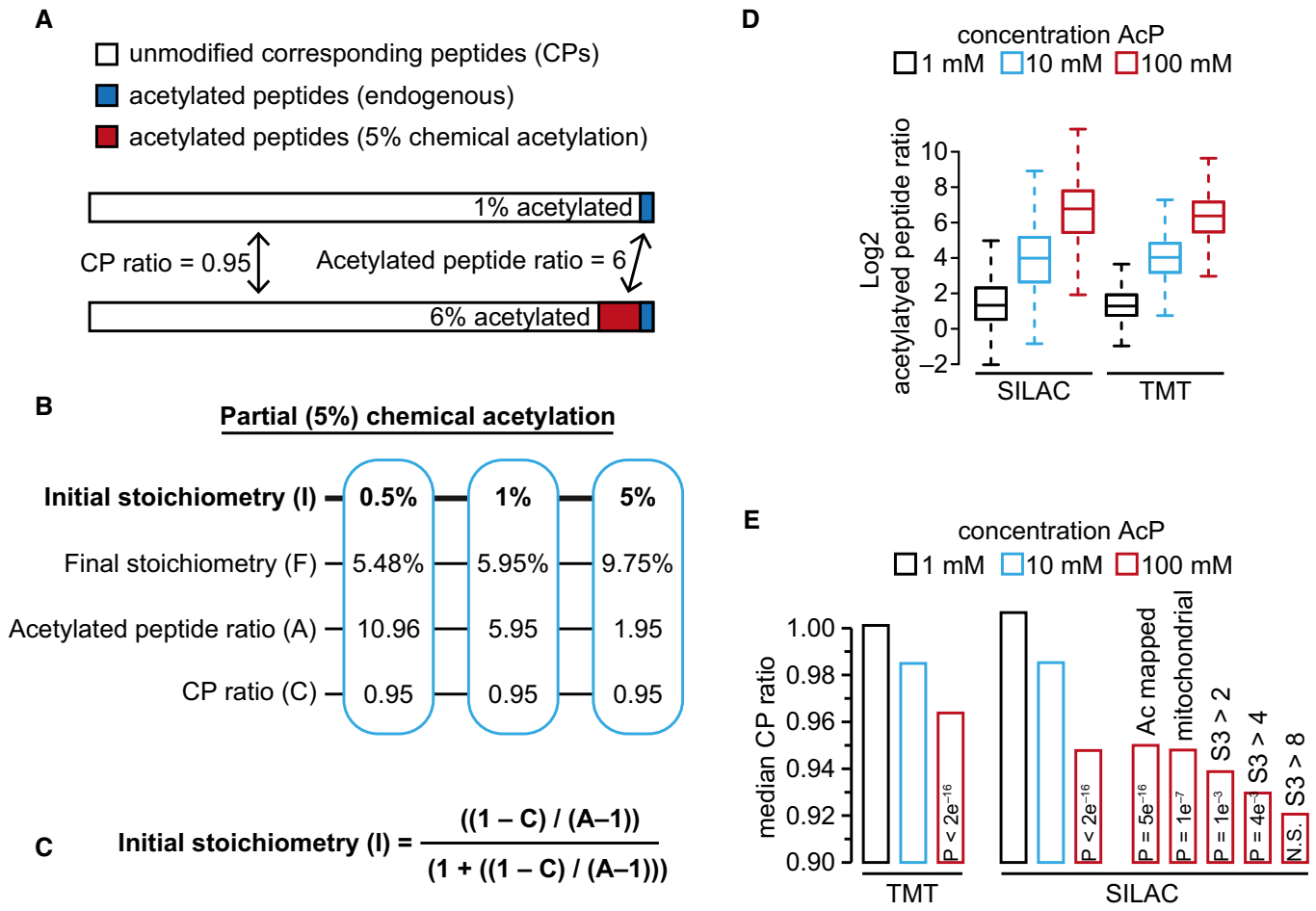

Figure 1. Estimating acetylation stoichiometry using partial chemical acetylation.

A Model illustrating the reciprocal relationship between acetylated peptides and their corresponding unmodified peptides (CPs) after 5% chemical acetylation. The diagram illustrates the relative amounts of unmodified and acetylated peptides occurring at an individual acetylation site; as acetylation increases, the amount of CPs is proportionally decreased.

B The table shows the relationship between acetylation stoichiometry, acetylated peptide ratio, and CP ratio after 5% chemical acetylation at the indicated initial acetylation stoichiometry.

C Equation used to calculate initial acetylation stoichiometry (I) based on acetylated peptide ratios (A) at individual sites measured in panel (D), and median CP ratios (C) measured in panel (E). The equation is derived from Olsen *et al* (2010).

D Acetyl phosphate (AcP) causes a concentration-dependent increase in acetylation. The box plots show the distributions of acetylated peptide ratios (AcP/control) quantified by SILAC or TMT. The box portion of the plot shows the interquartile range (IQR) and the line indicates the median value, whisker ends extend to 1.5 times the length of the IQR (unless the data range is smaller, in which case the whisker ends extend to the minimum or maximum value), outliers are not shown. Data is from a single experimental replicate that was performed independently for each quantitative method (SILAC or TMT).

E AcP causes a concentration-dependent, significant reduction in median CP abundance. The column graph shows median CP ratios based on an internally controlled comparison (see Materials and Methods). Ratios are for all CPs, unless indicated; sites where acetylation was mapped in this study (Ac mapped), sites on mitochondrial proteins (mitochondrial), or SIRT3-targeted sites [defined as having > 2-fold (S3 > 2), > 4-fold (S3 > 4), or > 8-fold (S3 > 8) increased acetylation in liver tissue from SIRT3 knockout (KO) mice (Hebert *et al*, 2013)]. Statistical significance was determined by Wilcoxon's test.

mice, see Fig 4), and liver tissue from four-month-old mice (Fig 2F). These mice were raised in independent animal facilities and their liver tissue harvested by different individuals. Therefore, our stoichiometry estimates appear to be generally applicable to diverse mouse liver tissues.

Stoichiometry of acetylation

Our measurements indicate that the vast majority of acetylation sites are modified at a very low stoichiometry. We calculated a median stoichiometry of acetylation that was ~0.05%. Mitochondrial sites had a significantly higher median stoichiometry (~0.11%) than non-mitochondrial sites (~0.04%) (Fig 3A), an observation that is consistent with our previous analysis in yeast cells (Weinert *et al*, 2014), and with the existence of separate mitochondrial and non-mitochondrial acetyl-CoA pools (Wellen *et al*, 2009). In yeast, high stoichiometry acetylation sites were associated with nuclear proteins involved in chromatin organization and transcription (Weinert *et al*, 2014). In this study, we estimated acetylation stoichiometry on a known regulatory site in the nucleus, structural

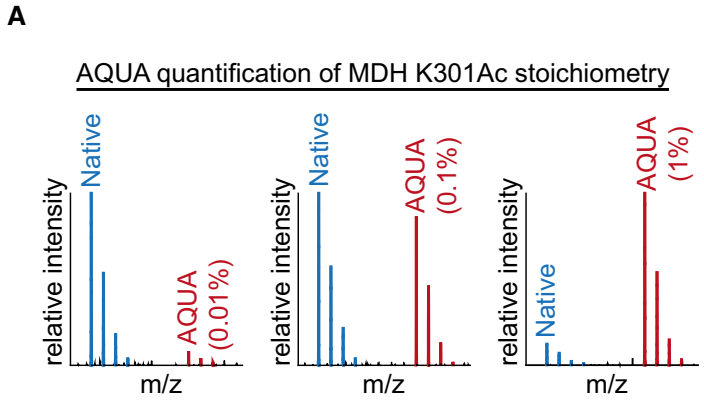

B

Protein name	Acetylated lysine	AQUA stoichiometry	SILAC stoichiometry	TMT stoichiometry
ACAT1	K260*	0.02%	0.01%	0.12%
HMGCS2	K310*	0.29%	0.70%	0.42%
HMGCS2	K447*	0.03%	0.04%	0.08%
MDH2	K239*	0.01%	N.D.	0.12%
MDH2	K301	0.13%	0.19%	0.18%
SDHA	K335*	0.02%	0.05%	0.05%
SDHA	K547	0.14%	0.33%	0.48%
SOD2	K68*	0.18%	0.86%	0.44%
SOD2	K122*	0.12%	0.30%	0.21%

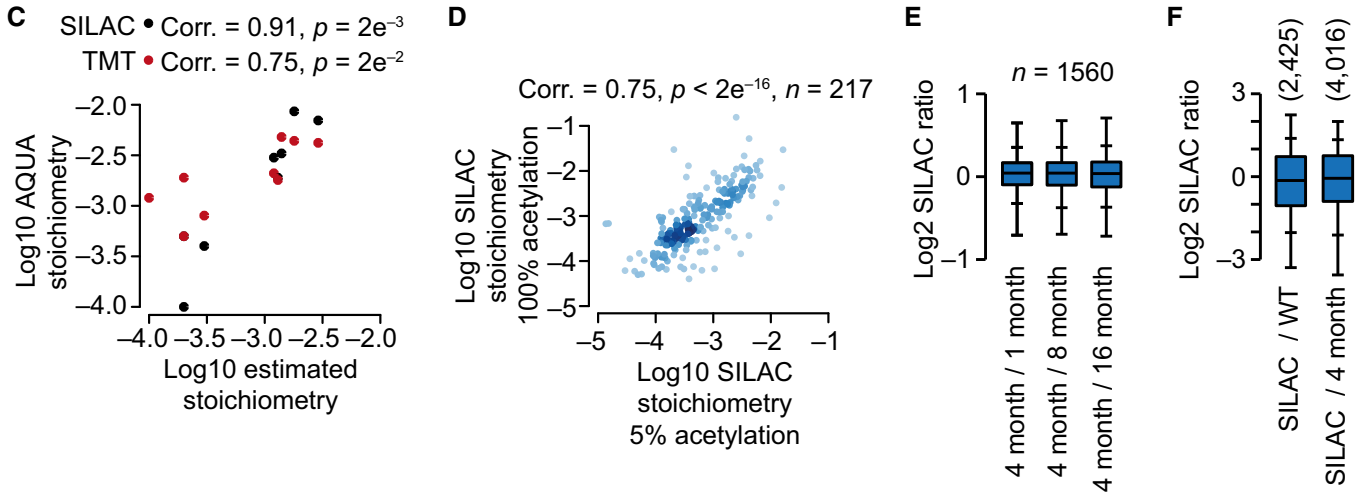

Figure 2. Validating estimated acetylation stoichiometry.

A The mass spectra show AQUA quantification of an endogenous acetylation site (MDH2 K301) using three dilutions (1%, 0.1%, and 0.01%) of AQUA peptide.

B Table comparing acetylation stoichiometry determined using AQUA peptides (AQUA stoichiometry) to estimates based on partial (5%) chemical acetylation using SILAC (SILAC stoichiometry) and TMT (TMT stoichiometry) quantification. AQUA stoichiometry is the median of two independent experimental replicates; SIRT3-targeted sites are indicated by * (see Appendix Table S1 for references).

C The scatterplot shows the correlation between AQUA stoichiometry and stoichiometry estimates based on partial chemical acetylation using either SILAC (black) or TMT (red) quantification. Spearman's correlation (Corr.) and *P*-value (p) by two-tailed test are shown.

D The scatterplot shows the correlation between estimated stoichiometry based on partial (5%) chemical acetylation and comprehensive (100%) chemical acetylation using SILAC quantification. Spearman's correlation (Corr.), *P*-value (p) by two-tailed test, and number (n) of estimates analyzed are shown.

E Acetylation levels are comparable in mice with different ages. The box plots show the distributions of acetylation site ratios comparing 4-month-old mice to 1-month-, 8-month-, and 16-month-old mice. Acetylation levels were compared using SILAC liver tissue as an internal standard for comparison; the number (*n*) of sites analyzed is shown. The box portion of the plot indicates the middle 50% of the distribution, inner hatch marks denote 9–91%, whisker ends 2–98%, and outliers are not shown.

F Acetylation levels are comparable in liver tissue from different mice. The box plots show acetylated peptide ratio distributions comparing SILAC liver tissue (SILAC) to liver tissue from an independent source (WT), and to the 4-month-old mice used to estimate acetylation stoichiometry in this study. Box plots are described in (E), the number of acetylated peptide SILAC ratios quantified are shown in parentheses.

maintenance of chromosomes protein 3 (SMC3) K106, which was 4% acetylated (Rolef Ben-Shahar *et al*, 2008; Zhang *et al*, 2008). However, most of the high stoichiometry sites we detected were on mitochondrial proteins, perhaps because the abundance of mitochondrial proteins in liver tissue limited the dynamic range of our analysis. Of the 4,322 sites with stoichiometry estimates, 344 occurred on proteins associated with the UniProt keyword "nucleus" while 1,532 occurred on proteins associated with the keyword "mitochondrion" (Dataset EV1). Although we detected known regulatory acetylation sites on histone N-terminal domains, these sites occurred on multiply acetylated peptides for which we were unable to accurately estimate stoichiometry and were therefore excluded from our analysis.

High stoichiometry acetylation (> 1% acetylated) was overrepresented on mitochondrial proteins; acyltransferases; lyases; butanoate metabolism; and valine, leucine, and isoleucine degradation

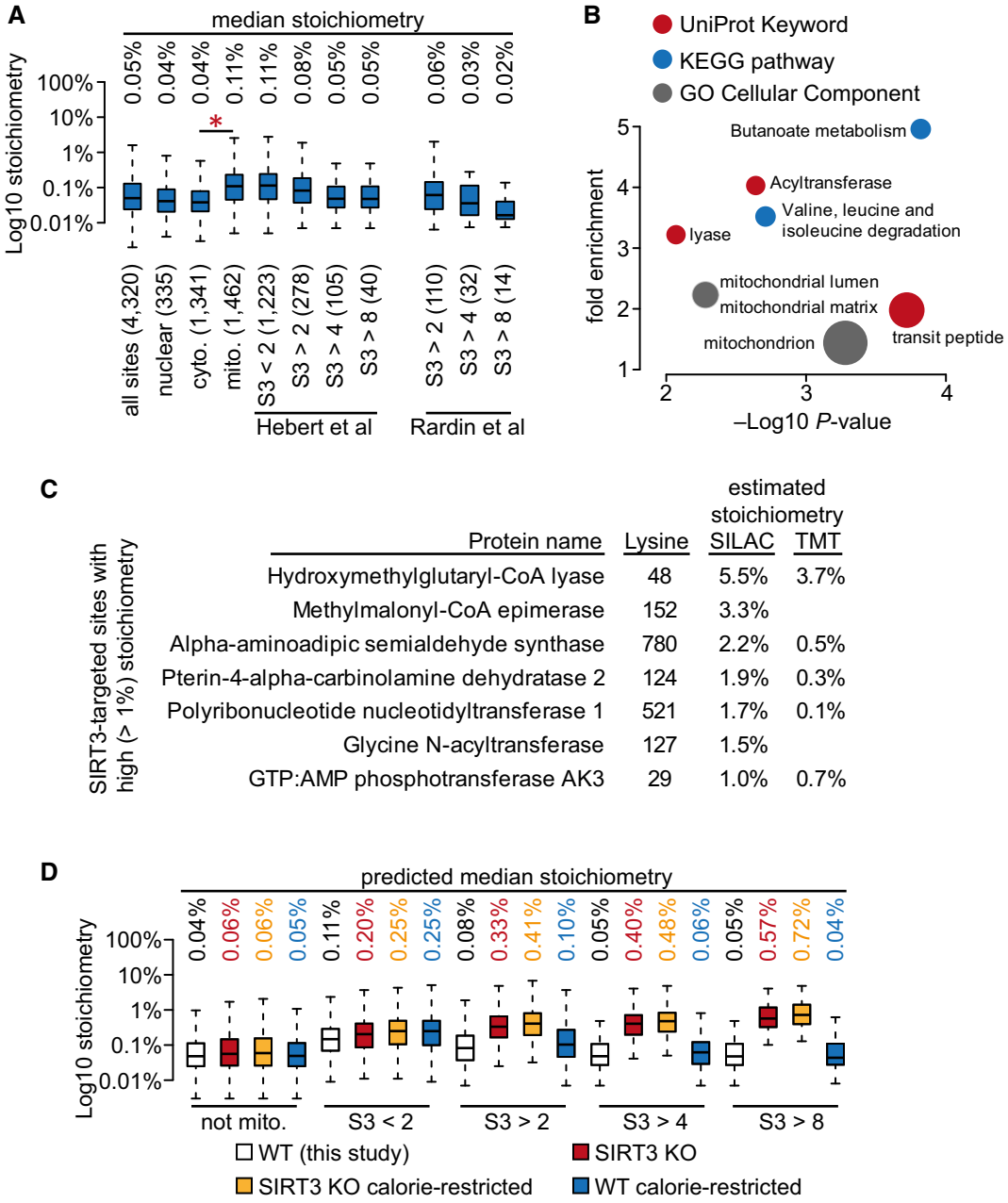

Figure 3. Acetylation stoichiometry.

A The box plots show the distributions of stoichiometry estimates based on partial (5%) chemical acetylation and SILAC quantification. The median stoichiometry of acetylation is shown above each box plot, and the number of sites analyzed is shown in parenthesis. Proteins were classified by association with the UniProt keywords "nuclear" (nuclear), "cytoplasmic" (cyto.), or "mitochondrion" (mito.). SIRT3-targeted sites were classified based on the degree of increased acetylation in SIRT3 KO liver tissue (Hebert *et al*, 2013); untargeted sites (S3 < 2) and sites with > 2-fold (S3 > 2), > 4-fold (S3 > 4), or > 8-fold (S3 > 8) increased acetylation are shown. SIRT3-targeted sites were additionally classified based on the degree of increased acetylation in SIRT3 KO liver tissue (Rardin *et al*, 2013b); sites with > 2-fold (S3 > 2), > 4-fold (S3 > 4), or > 8-fold (S3 > 8) increased acetylation are shown. Significance was determined by Wilcoxon's test (*$P < 2e^{-16}$).

B Gene Ontology enrichment analysis of proteins harboring high stoichiometry (> 1%) acetylation sites. The scatterplot shows the significance of GO term enrichment (-Log10 *P*-value) and the degree of GO term enrichment (fold enrichment) comparing proteins with high stoichiometry (> 1%) sites to proteins with low stoichiometry (< 1%) sites. The size of each point is proportional to the number of proteins associating with the term.

C Proteins with high stoichiometry (> 1%), SIRT3-targeted acetylation sites. The table lists the estimated stoichiometry based on partial (5%) chemical acetylation using either SILAC or TMT quantification for SIRT3-targeted sites (defined as having > 2-fold increased acetylation in SIRT3 KO liver tissue (Hebert *et al*, 2013)).

D The box plots show the distributions of stoichiometry estimates based on SILAC quantification. Acetylation sites were classified as in (A). Stoichiometry was predicted in SIRT3 knockout (KO), calorie-restricted SIRT3 KO mice, and calorie-restricted wild-type (WT) mice using the acetylation changes quantified by Hebert *et al* (2013). The median predicted stoichiometry of acetylation is shown above each box plot.

Data Information: (A, D) The box portion of the plot shows the interquartile range (IQR) and the line indicates the median value, whisker ends extend to 1.5 times the length of the IQR (unless the data range is smaller, in which case the whisker ends extend to the minimum or maximum value), outliers are not shown.

(Fig 3B). Overrepresentation of high stoichiometry acetylation sites on mitochondrial proteins is consistent with our observation of significantly higher median stoichiometry in this organelle (Fig 3A). We further observed that high stoichiometry sites were frequently found on enzymes that catalyze reactions involving acetyl groups, such as AACS (K391, 13% acetylated), NAA30 (K235, 8% acetylated), NAA50 (K34, 5% acetylated), ACSM1 (K200, 5% acetylated), KEG1 (K128, 4% acetylated), and GLYAT (K127, 1.5% acetylated). These findings suggest that enzymes that transfer acetyl groups may accumulate higher levels of acetylation due to autocatalysis or higher local concentrations of acetyl metabolites. A recent study similarly found that acetyl-CoA acetyltransferase 1 (ACAT1) catalyzed lysine acetylation of pyruvate dehydrogenase (PDHA1) K321 and pyruvate dehydrogenase phosphatase (PDP1) K202, mediating the Warburg effect in EGF-treated and immortalized cells (Fan *et al*, 2014). We determined acetylation stoichiometry at PDHA1 K321 by SILAC (0.84% acetylated) and TMT (0.39% acetylated). The low stoichiometry found at this position in liver tissue is consistent with the idea that PDHA1 K321 acetylation is only found after EGF stimulation or in immortalized cell lines (Fan *et al*, 2014).

We also estimated acetylation stoichiometry at more than 20 sites that were previously suggested to regulate metabolic proteins (Appendix Table S1), and found that nearly all of these sites were < 1% acetylated. Stoichiometry at several of these positions was independently determined using the AQUA method (Fig 2B), providing additional confidence in these findings. Our results differ from a previous study that reported high stoichiometry acetylation on enoyl-coenzyme A hydratase (EHHADH) and malate dehydrogenase (MDH2) (Zhao *et al*, 2010). While the reasons for these differences are not clear, it is plausible that the levels of acetylation may be different in the analyzed samples. In the study from Zhao *et al*, EHHADH and MDH2 were expressed ectopically in cultured cells, while we estimated acetylation stoichiometry on the endogenously expressed proteins in liver tissue.

Acetylation stoichiometry at SIRT3-targeted sites

Acetylation stoichiometry at SIRT3-targeted sites (S3 > 2, median 0.08%) was slightly lower than at mitochondrial sites not targeted by SIRT3 (S3 < 2, median 0.11%), while the sites most affected in SIRT3 KO mice (S3 > 4, S3 > 8) had even lower median stoichiometry (0.05%) (Fig 3A). For these analyses, we used SIRT3-targeted sites defined by Hebert *et al* (2013); however, estimated stoichiometry was similar if we used SIRT3-targeted sites defined in an independent study that used a different quantitative method (Rardin *et al*, 2013b) (Fig 3A). These data indicate that SIRT3 suppresses acetylation to background levels at targeted sites. While the vast majority (97%) of SIRT3-targeted sites were < 1% acetylated, some SIRT3-targeted sites were acetylated at a high (> 1%) stoichiometry (Fig 3C).

SIRT3-deficient animals have reduced metabolic function, which is linked to increased mitochondrial protein acetylation. In order to systematically investigate acetylation stoichiometry in SIRT3-deficient animals, we used previously determined changes in liver protein acetylation in SIRT3 KO, calorie-restricted SIRT3 KO, and calorie-restricted wild-type mice (Hebert *et al*, 2013) to predict acetylation stoichiometry under these conditions (Fig 3D and Dataset EV1). SIRT3-targeted sites (S3 > 2) were predicted to have a median 4-fold increase in acetylation stoichiometry in SIRT3 KO animals, and this increase was slightly greater (5-fold) in calorie-restricted SIRT3 KO animals. Sites that were most affected by loss of SIRT3 (S3 > 8) were predicted to have the greatest increase in acetylation stoichiometry, ~11-fold in SIRT3 KO animals and ~20-fold in calorie-restricted SIRT3 KO animals (Fig 3D). Glycine N-acyltransferase (GLYAT) K127 is ~57-fold elevated in both fed and calorie-restricted SIRT3 KO animals (Hebert *et al*, 2013). We estimated that this lysine is ~1.5% acetylated in wild-type animals, suggesting that acetylation stoichiometry could be as high as 87% in the absence of SIRT3. In addition, we predicted that hydroxymethylglutaryl-CoA lyase (HMGCL) K48 is ~16% acetylated and methylmalonyl-CoA epimerase (MCEE) K152 is ~9% acetylated in SIRT3 KO animals. In total, 48 SIRT3-targeted sites were predicted to have high (> 1%) stoichiometry in SIRT3 KO animals and 57 SIRT3-targeted sites were predicted to have high stoichiometry in calorie-restricted SIRT3 KO animals. In contrast, only 13 SIRT3-targeted sites were predicted to have high stoichiometry in calorie-restricted wild-type animals. SIRT3-targeted sites were not substantially altered by calorie restriction in wild-type animals; therefore, the stoichiometry we predicted at these sites was similarly unaltered (Fig 3D, compare WT to WT calorie-restricted). Notably, sites not targeted by SIRT3 were slightly increased (median 2.3-fold) by calorie restriction in wild-type animals, while the median stoichiometry of SIRT3-targeted sites was unchanged. These analyses suggest that acetylation reaches a sufficient stoichiometry in SIRT KO animals to account for the metabolic defects seen in these animals, particularly if multiple proteins and acetylation sites are affected in a common metabolic pathway.

Acetylation at SIRT3-targeted sites is mostly unaffected by fasting

Given the low stoichiometry of acetylation at SIRT3-targeted sites, understanding how acetylation at these positions is affected by dietary manipulations is important for determining whether SIRT3 regulates mitochondrial proteins by deacetylating SIRT3-targeted sites in response to dietary changes. In order to examine how fasting affects acetylation at SIRT3-targeted sites, we measured acetylation levels after fasting, and after fasting in a genetic mouse model that is deficient in generating fatty acids (FAs). Fasting triggers the mobilization of FAs from adipose tissues to the liver, where they are oxidized to acetyl-CoA in mitochondria. Adipose triglyceride lipase (ATGL) is important for lipolysis in adipose tissues, and ATGL-deficient mice have a reduced capacity to generate FAs for energy homeostasis (Haemmerle *et al*, 2006; Zimmermann *et al*, 2009). We used SILAC liver tissue to quantify acetylation levels in fed and fasted, wild-type and ATGL-deficient mouse liver tissue (Dataset EV5). Since we used the same SILAC liver tissue that was used to estimate stoichiometry in our previous experiments, we could directly estimate acetylation stoichiometry in these animals and found that stoichiometry in fed wild-type mice was comparable to our previous estimates (Appendix Fig S3). Fasting caused globally (median 1.8-fold) increased acetylation of mitochondrial proteins in liver tissue, and this effect was significantly abrogated in ATGL-deficient animals (Fig 4A). Notably, the effect of fasting on mitochondrial acetylation was significantly greater at SIRT3-targeted sites in a manner that was proportional to the effect of SIRT3 deficiency on these sites (Fig 4A), mirroring the greater sensitivity of these sites to partial chemical acetylation (Fig 1E). ATGL-deficiency partially

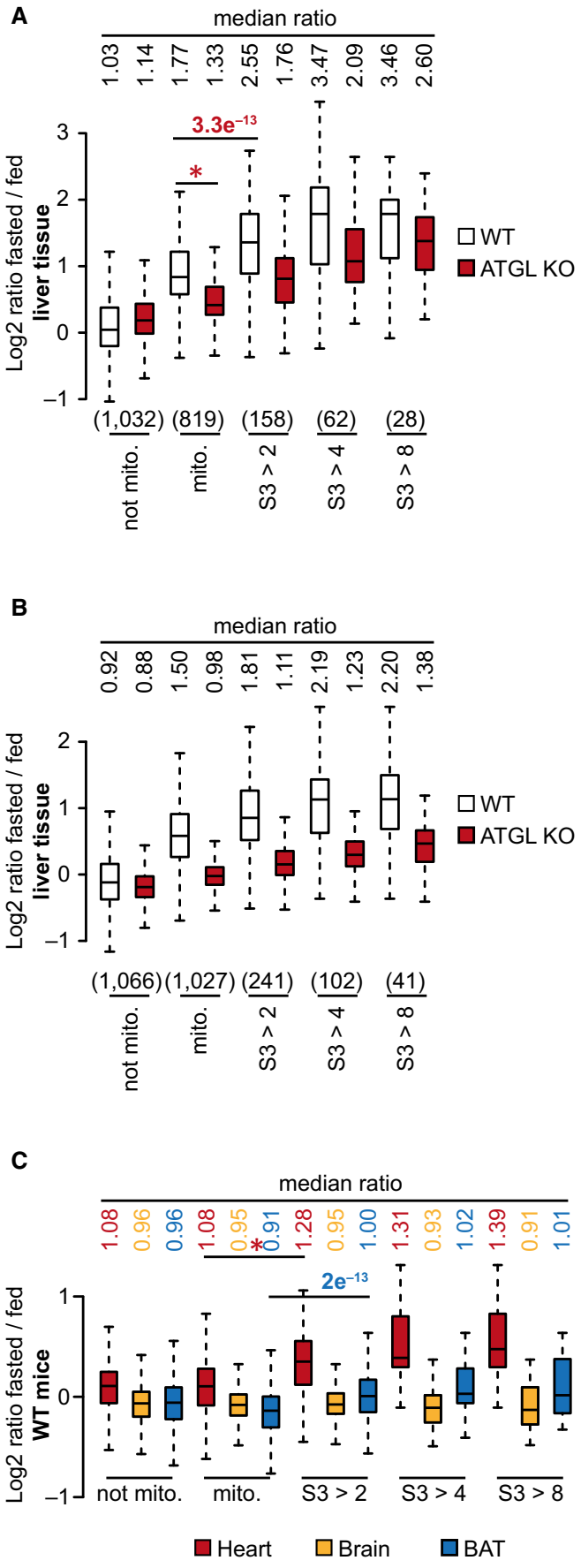

Figure 4. Fasting-induced acetylation in mouse tissues.

A The box plots show the distribution of acetylation site ratios comparing the liver tissues of fasted mice to fed mice. Differences in acetylation were quantified using SILAC. Significance was determined by Wilcoxon's test (*P*-values shown in red, $*P < 2e^{-16}$). Proteins were classified by association with the UniProt keyword "mitochondrial" (mito.). SIRT3-targeted sites were classified based on the degree of increased acetylation in SIRT3 KO liver tissue (Hebert *et al*, 2013); untargeted sites (S3 < 2) and sites with > 2-fold (S3 > 2), > 4-fold (S3 > 4), or > 8-fold (S3 > 8) are shown. Numbers of quantified sites are shown in parenthesis, and the median ratio is shown above each box plot.

B The box plots show essentially the same experiment as shown in (A) except that differences in acetylation were quantified using TMT.

C The box plots show the distribution of acetylation site ratios comparing the heart, brain, and brown adipose tissue (BAT) of fasted mice to fed mice. Differences in acetylation were quantified using TMT. Sites were classified as in (A). Significance was determined by Wilcoxon's test ($*P < 2e^{-16}$). Although not indicated in the figure panel, sites most affected by SIRT3 were significantly increased by fasting in heart tissue (S3 > 4, *P* = 6e-15; S3 > 8, *P* = 5e-8) and BAT (S3 > 4, *P* = 4e-10; S3 > 8, *P* = 5e-4) when compared to mitochondrial sites. Acetylation in brain tissue was not significantly different.

Data Information: (A–C) The box portion of the plot shows the interquartile range (IQR) and the line indicates the median value, whisker ends extend to 1.5 times the length of the IQR (unless the data range is smaller, in which case the whisker ends extend to the minimum or maximum value), outliers are not shown.

suppressed increased mitochondrial acetylation, both at untargeted and at SIRT3-targeted sites, suggesting that FA oxidation drives increased mitochondrial acetylation in the liver tissue of fasted animals. We verified that SIRT3 was similarly expressed in the liver tissue of fed and fasted, wild-type and ATGL KO mice (Appendix Fig S4), suggesting that differences in acetylation at SIRT3-targeted sites were unlikely to result from differences in SIRT3 protein abundance.

We verified these findings in liver tissue using TMT quantification (Fig 4B and Dataset EV6) and additionally used TMT to quantify acetylation changes in heart, brain, and brown adipose tissue (BAT) (Fig 4C and Dataset EV6). TMT quantification revealed similar changes in liver acetylation, although the magnitude of these changes was not as great as seen with SILAC quantification (Fig 4B). The greater sensitivity of SIRT3-targeted sites to fasting-induced acetylation was also seen in heart tissue where fasting only caused significantly increased acetylation at SIRT3-targeted sites (Fig 4C). In brain and BAT, fasting did not result in substantially altered acetylation (note that the vast majority of sites are < 2-fold affected by fasting, Fig 4C), although median acetylation levels were slightly, but significantly, higher at SIRT3-targeted sites in fasted BAT.

A previous study examined acetylation dynamics in the liver tissue of calorie-restricted wild-type and SIRT3 KO mice (Hebert *et al*, 2013), and their data showed that SIRT3-targeted acetylation sites were mostly unchanged in calorie-restricted, wild-type animals (Fig 3C and Appendix Fig S5A). Another study examining liver acetylation in fasted and obese mice (Still *et al*, 2013) showed that median acetylation levels were not substantially altered by fasting or obesity in wild-type animals (Appendix Fig S5B). A small number of acetylation sites were significantly affected by fasting and obesity (Still *et al*, 2013), and our analysis of their data showed that SIRT3-targeted sites were the most affected by fasting (Appendix Fig S5B), consistent with our own results (Fig 4A and B). Together, these data

suggest that SIRT3-targeted sites are only modestly affected by fasting or calorie restriction, in contrast to the substantially increased acetylation seen in SIRT3 KO animals (Hebert *et al*, 2013; Rardin *et al*, 2013b). In particular, induction of SIRT3 activity should reduce acetylation at these positions, while we observed modestly increased acetylation in liver and heart tissues. This suggests that SIRT3 is unable to completely suppress fasting-induced acetylation at these positions. Interestingly, while calorie restriction and fasting cause a similar global increase in mitochondrial acetylation in liver tissue (Schwer *et al*, 2009; Hebert *et al*, 2013; Pougovkina *et al*, 2014), acetylation at SIRT3-targeted sites remains mostly unchanged in calorie-restricted wild-type animals (Fig 3D, Appendix Fig S5A). This suggests that acute fasting has a more robust effect on SIRT3-targeted sites than prolonged calorie restriction, perhaps because SIRT3 expression was not sufficiently induced at this time point.

SIRT3 has a greater impact on acetylation levels in tissues

In a recent study, we showed that acetylation accumulated in the mitochondria of metabolically active, growth-arrested yeast cells (Weinert *et al*, 2014). We similarly found that mitochondrial acetylation accumulates in growth-arrested, serum-starved human cervical cancer (HeLa) cells (Fig 5A), and we reasoned that acetylation might similarly accumulate in the metabolically active, postmitotic cells of metazoans. In order to test this idea, we used a SILAC-based MS approach to compare acetylation in two different exponentially growing mouse embryonic fibroblast (MEF) cell lines to four different mouse tissues. Acetylation levels, corrected for differences in protein abundance between cells and tissues, were higher in all four tissues (Fig 5B and Dataset EV7). Notably, mitochondrial protein acetylation was significantly higher than non-mitochondrial acetylation, mirroring the effect of growth arrest on yeast (Weinert *et al*, 2014) and HeLa cells (Fig 5A). We suspect that growth arrest causes increased acetylation by prolonging the exposure of proteins to acetyl-CoA; however, the precise mechanism remains unclear, and it is possible that other physiological differences between cultured MEF cells and tissues result in higher levels of mitochondrial acetylation in tissues. Regardless, the observed elevated mitochondrial protein acetylation in tissues suggests that the function of SIRT3 in suppressing acetylation may have a greater impact in the context of tissues. In order to test this idea, we compared previously published proteomics data identifying SIRT3-targeted sites in MEFs (Sol *et al*, 2012), and liver tissue (Hebert *et al*, 2013), and found that loss of SIRT3 affected acetylation to a greater degree in liver tissue than in MEFs (Fig 5C). These data illustrate the idea that the impact of SIRT3 deficiency may depend on the propensity of the cell type or tissue to accumulate acetylation, which will be similarly impacted by the metabolic state.

Discussion

In this work, we investigated the stoichiometry of lysine acetylation in mouse liver tissue with a particular focus on SIRT3-targeted acetylation sites. We found that most acetylation occurs at a very low stoichiometry, including SIRT3-targeted sites and other putative regulatory sites. We further found that the majority of SIRT3-targeted sites are mostly unaffected by fasting. Our findings support an emerging model whereby most acetylation occurs nonenzymatically and SIRT3 has a major function in protecting metabolic fidelity by suppressing acetylation on mitochondrial proteins.

Nonenzymatic acetylation

Recent studies suggest that most acetylation occurs nonenzymatically through exposure to acetyl-CoA, particularly in the high pH

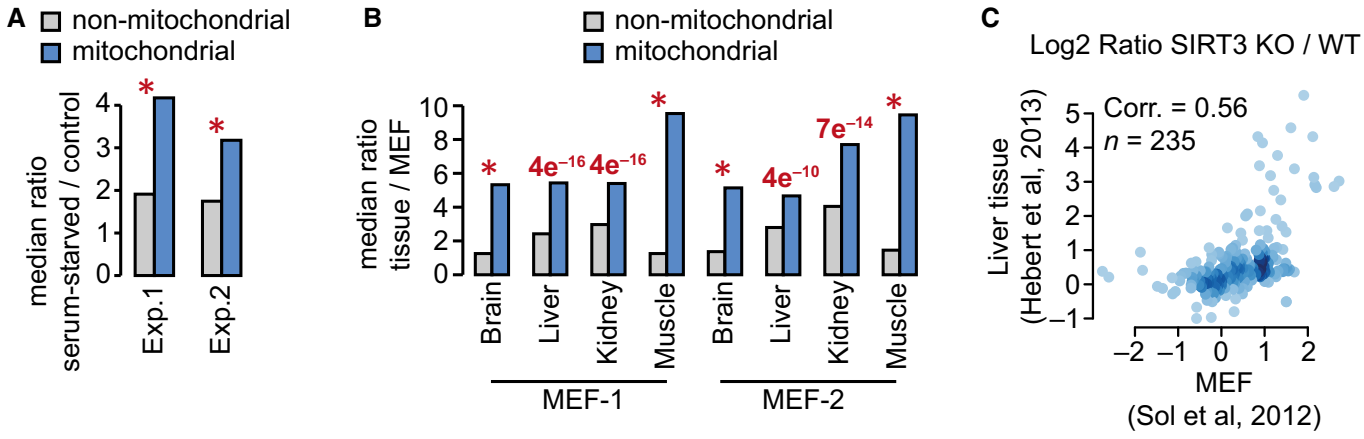

Figure 5. Acetylation levels are higher, and the impact of SIRT3-deficiency is greater, in tissues than in cultured cells.

A Acetylation accumulates in the mitochondria of serum-starved human cervical cancer (HeLa) cells. The bar graphs show the median ratio comparing serum-starved to control, exponentially dividing cells. Mitochondrial proteins were classified based on association with the UniProt keyword "Mitochondrion."

B Acetylation accumulates in tissues. The column graph shows the median ratio of acetylation comparing two mouse embryonic fibroblast cell lines (MEF-1 and MEF-2) to four different mouse tissues. Mitochondrial protein classification as in (A).

C SIRT3 has a greater effect on acetylation levels in liver tissue compared to MEFs. The scatterplot shows the correlation between acetylation sites quantified in SIRT3 KO liver tissue (Hebert *et al*, 2013) and MEF cells (Sol *et al*, 2012). The Spearman's correlation (Corr.) and number of sites compared (n) are shown.

Data information: (A, B) Significance was determined by Wilcoxon's test (*P*-values shown in red, $*P < 2e^{-16}$).

environment of the mitochondrial matrix (Wagner & Payne, 2013; Weinert *et al*, 2014). Here we showed that liver mitochondrial protein acetylation occurs at a significantly higher stoichiometry than cytoplasmic and nuclear protein acetylation. These findings are consistent with a separate mitochondrial acetyl-CoA pool and high pH environment that favors nonenzymatic acetylation. We additionally found that fasting-induced mitochondrial acetylation was abrogated by loss of ATGL, suggesting that FA oxidation promotes mitochondrial protein acetylation. An independent study reported that fasting-induced mitochondrial acetylation in liver tissue depended on very-long-chain acyl-CoA dehydrogenase (VLCAD), a central enzyme in FA oxidation (Pougovkina *et al*, 2014). Pougovkina *et al* further showed that inducing fatty acid oxidation in fibroblasts increases protein acetylation and that fatty acids are a direct source for mitochondrial protein acetylation. These results are consistent with the idea that acetyl-CoA, formed through FA oxidation, impacts mitochondrial acetylation levels by a nonenzymatic mechanism. Furthermore, nonenzymatic acetylation is consistent with the global changes in mitochondrial acetylation caused by fasting and loss of ATGL and is consistent with the low stoichiometry of acetylation.

SIRT3: protein regulator or protein repair factor?

Many studies have shown that SIRT3 deficiency results in increased mitochondrial acetylation and reduced activity of numerous mitochondrial enzymes (Newman *et al*, 2012). SIRT3 protein levels are increased upon fasting and calorie restriction (Shi *et al*, 2005; Palacios *et al*, 2009; Hirschey *et al*, 2010; Tao *et al*, 2010; Newman *et al*, 2012), and increased SIRT3 activity has been suggested to regulate metabolism under these conditions. However, with the exception of a single study (Fan *et al*, 2014), a regulatory axis between enzyme-catalyzed acetylation and SIRT3-mediated deacetylation has not been demonstrated. A hallmark of protein regulation by posttranslational modifications is site-specific, enzyme-catalyzed modification that mostly occurs in a conditional manner. However, there is little evidence of enzyme-catalyzed, site-specific acetylation in mitochondria, and several studies suggest that most mitochondrial acetylation occurs nonenzymatically (Wagner & Payne, 2013; Pougovkina *et al*, 2014; Weinert *et al*, 2014). Based on these observations, a recent review suggested that SIRT3 protects mitochondrial protein activity by suppressing nonenzymatic acetylation (Wagner & Hirschey, 2014).

The results presented in this study provide support for the idea that SIRT3 repairs nonenzymatic acetylation lesions on mitochondrial proteins in order to preserve their normal function. Most importantly, we found that SIRT3 suppressed acetylation to a very low stoichiometry at targeted sites. This suggests that SIRT3 is unlikely to regulate protein function by further deacetylating mitochondrial proteins, as the stoichiometry of acetylation is already very low, and acetylation at SIRT3-targeted sites typically inhibits enzymatic activity (Lin *et al*, 2012; Ghanta *et al*, 2013). We found that fasting did not result in reduced acetylation at SIRT3-targeted sites and these findings are consistent with the previously published proteome-wide studies investigating mitochondrial acetylation in calorie-restricted, fasted, and obese mice (Hebert *et al*, 2013; Still *et al*, 2013). In light of our stoichiometry estimates, these results indicate that these dietary manipulations do not substantially alter acetylation levels at SIRT3-targeted sites generally. In contrast, loss of SIRT3 results in substantially increased acetylation at targeted sites that exceeds any changes observed at these same sites in fasted, calorie-restricted, or obese wild-type animals, indicating that the role of SIRT3 in suppressing acetylation is greater than the effect of dietary manipulations on acetylation levels at these sites (e.g., see Fig 3D). We found that SIRT3-targeted sites were similarly sensitive to fasting-induced acetylation *in vivo* and nonenzymatic acetylation *in vitro*, in a manner that was proportional to the degree of increased acetylation in SIRT3 KO animals. These data suggest that the increased acetylation at these sites in the absence of SIRT3 is a function of their inherent reactivity and the nonenzymatic origin of acetylation. This idea is further supported by our observation that fasting-induced acetylation at SIRT3-targeted sites was suppressed by loss of ATGL. Together, our data indicate that SIRT3 suppresses acetylation to a very low stoichiometry under all conditions analyzed, and suggest that a constitutive function of SIRT3 is to remove nonenzymatic acetylation lesions from mitochondrial proteins. The mitochondrial sirtuin deacylase SIRT5 suppresses both succinylation and glutarylation in mitochondria (Du *et al*, 2011; Park *et al*, 2013; Rardin *et al*, 2013a; Tan *et al*, 2014), and both of these modifications may occur nonenzymatically (Wagner & Payne, 2013; Weinert *et al*, 2013b; Tan *et al*, 2014), suggesting that sirtuin deacylases may have a general role in protecting mitochondrial proteins from reactive acyl-CoA metabolites.

It is important to note that our data and their implications are global in nature; we describe the general properties of acetylation sites that are affected by SIRT3 deficiency. SIRT3 may have a general function in suppressing nonenzymatic acetylation, as our data suggest, and also have specific functions in regulating individual sites, as suggested in previous studies. Furthermore, it may be possible that nonenzymatic acetylation and SIRT3 deacetylation combine to regulate metabolism in a physiologically relevant manner. Of particular interest may be conditions that inhibit SIRT3 activity (Jing *et al*, 2013), allowing acetylation to accumulate at targeted sites. However, future work needs to consider the stoichiometry of acetylation when determining whether acetylation regulates protein function, in particular for metabolic enzymes where site-specific acetylation is thought to impair their catalytic efficiency.

Materials and Methods

Sample preparation

All mouse work was performed according to national and international guidelines approved by the Danish Animal Ethical Committee and the Review Board at the Faculty of Health and Medical Sciences, University of Copenhagen. ATGL-deficient and isogenic wild-type mice were handled according to the guidelines of the Federation of European Laboratory Animal Science and were approved by Austrian government authorities. Mouse liver tissues used for stoichiometry estimation (from 1-, 4-, 8-, and 16-month-old animals) were harvested mid-morning from five 16-week C57BL/6 male mice fed ad libitum and transferred immediately to liquid nitrogen. A total of 8- to 10-week-old male wild-type and ATGL-deficient animals (both on C57BL/6J background) were sacrificed and tissues immediately snap-frozen in pre-chilled 2-methylbutane and stored

in liquid nitrogen. Tissues from several mice were pooled and pulverized at −180°C using a liquid nitrogen chilled Retsch MM 400 Ball Mill, mixed with lysis buffer (50 mM Tris, pH 7.5, 150 mM NaCl, 1 mM EDTA, 1% NP-40, 0.1% sodium deoxycholate, 1× complete protease inhibitor cocktail (Roche), 10 mM nicotinamide, 5 mM valproic acid), clarified by centrifugation, and precipitated with −20°C acetone. Mouse embryonic fibroblast (MEF) and HeLa cell lines were cultured in DMEM (PAA Laboratories) supplemented with heavy isotopes of arginine and lysine ($^{13}C_6{}^{15}N_4$-arginine and $^{13}C_6{}^{15}N_2$-lysine, Cambridge Isotope Laboratories) and dialyzed serum (Sigma). All cell lines were tested for mycoplasma infection before use. HeLa cells were serum-starved for 48 hours by washing the cells twice with PBS before transferring into the above-described DMEM lacking dialyzed serum. Cells were harvested using lysis buffer (above) and centrifuged, and protein was acetone-precipitated. Acetone-precipitated protein was re-dissolved in urea solution (6M urea, 2M thio-urea, 10 mM Hepes pH 8.0), and the concentration was determined by Quick-Start Bradford assay (Bio-Rad). Protein was treated with freshly prepared acetyl phosphate (AcP, Sigma) in urea solution at 37°C for 3 h. AcP was removed by acetone precipitation. Protein digestion, peptide purification, acetyllysine peptide enrichment, and SCX fractionation were performed as described (Weinert *et al*, 2013a).

Mass spectrometry

Peptide fractions were analyzed by online nanoflow LC-MS/MS using a Proxeon easy nLC system connected to an LTQ Orbitrap Velos or Q-Exactive mass spectrometer (Thermo Scientific), as described (Kelstrup *et al*, 2012; Weinert *et al*, 2013a). Raw data was computationally processed using MaxQuant (version 1.5.2.8) and searched against the UniProt database (downloaded on January 23, 2014) using the integrated Andromeda search engine (http://www.maxquant.org/) (Cox *et al*, 2011). Acetylation sites were further filtered to ensure a localization probability greater than 90%, and to remove redundant entries. In order to reduce parent ion interference, quantification using TMT reporter ions was performed using only fragment (MS2) scans where the targeted ion constituted more than 75% of the total ions present (parent ion fraction, PIF > 0.75). All sites quantified by SILAC in this study were detected in untreated control samples, indicating that these sites occurred endogenously in the absence of chemical acetylation. Similarly, sites quantified by TMT had reporter ion signal in untreated control samples. Only singly acetylated peptides were used for estimating stoichiometry; peptides with more than one acetylation sites were omitted because it was not possible to account for different degrees of initial stoichiometry at each individual position. The experimental setup used in all quantitative MS experiments can be found in Appendix Table S2. The raw data and MaxQuant output files have been deposited to the ProteomeXchange Consortium (http://proteomecentral.proteomexchange.org) via the PRIDE partner repository (Vizcaino *et al*, 2013) with the dataset identifier PXD000885.

Measuring median unmodified corresponding peptide ratios

At a low degree of chemical acetylation, the small decrease in CP abundance (predicted ratio of 0.95 for 5% chemical acetylation) was not resolvable for individual peptides. In order to overcome this limitation, we examined the median ratio of thousands of peptides in an internally controlled comparison, which provided statistically significant differences. Trypsin cleaves proteins C-terminal to lysine and arginine, but it is unable to cleave at acetylated lysine residues. Since we chemically acetylated our proteins under denaturing conditions, all tryptic peptides generated by cleaving a lysine residue will be reduced in a manner that is proportional to the degree of acetylation. Arginine-flanked (AF) peptides (generated by cleavage at two arginine residues) will be unaffected by acetylation, while the cleavage of lysine-dependent (LD) peptides (generated by cleavage at one lysine and one arginine) and lysine-flanked (LF) peptides (generated by cleavage at two lysines) will be blocked by acetylation. LF peptides are twice as likely to be blocked by acetylation as LD peptides, since acetylation can block peptide cleavage at either lysine. Since SILAC samples were only lysine-labeled, we calculated median CP ratios by taking the median ratio of LF peptides relative to LD peptides. However, for TMT samples the relative decreases seen comparing LF to LD peptides were consistent with that seen comparing LD to AF peptides.

AQUA quantification

AQUA was performed using AQUA QuantPro heavy-isotope-labeled peptide standards (Thermo Fisher Scientific). Native acetylated peptides could not be detected without enrichment of acetylated peptides (we estimated our detection limit for these peptides to be ~1% stoichiometry). In order to overcome the detection limit, we devised a strategy to combine AQUA peptides with affinity enrichment. First, we determined protein abundances for our proteins of interest using AQUA quantification of unmodified peptides (one unmodified peptide for each protein, see Dataset EV3 for AQUA peptide sequences). AQUA peptides were serially diluted, and the AQUA peptide dilution with the closest intensity to the native peptide was used for quantification with a minimum of three independent measurements. Acetylated AQUA peptides were then spiked into the liver peptide preparation at three concentrations (in separate reactions) to yield final stoichiometry of 1%, 0.1%, or 0.01%. Different amounts of each AQUA peptide were added according to the individual protein abundances in the peptide preparation. Acetylated peptides were then affinity-enriched to enable detection of the acetylated native and acetylated AQUA peptides. All three concentrations of acetylated AQUA peptides (1%, 0.1%, and 0.01% stoichiometries) were used for quantification in technical duplicate measurements (6 measurements in total), and the experiment was performed in two independent runs.

Quantifying stoichiometry using 100% acetylation

SILAC liver protein was 100% acetylated in 8M guanidine HCl, 50 mM Hepes pH 8.5 using 40 mM NHS-acetate (Thermo Scientific) for 2 h at room temperature, and the reaction was quenched with 200 mM Tris, pH 7.5. Hundred percent acetylated SILAC protein was mixed with unlabeled liver protein from 4-month-old male mice to 1%, 0.1%, or 0.01% stoichiometry. Acetylated peptides were enriched from these samples, and acetylation stoichiometry was calculated by dividing the stoichiometry of mixing (1%, 0.1%, or

0.01%) by the SILAC ratio. For example, if 100% acetylated SILAC protein was added at a 1/100 dilution (1%), we divided 1% by the SILAC ratio to calculate stoichiometry. Estimating stoichiometry using 100% acetylation is limited to peptides generated by cleavage at arginine residues, thereby resulting in far fewer stoichiometry estimates than our method using partial chemical acetylation. In our data analysis, we only considered acetylation site ratios quantified from peptides generated by cleaving arginine residues.

A number of important controls were performed. Hundred percent acetylation was confirmed by comparing the number of lysine-dependent tryptic peptides recovered in 100% acetylated ($n = 16$) and control samples ($n = 713$), confirming that acetylation caused a 98% reduction in these peptides. In order to control for efficient tryptic digestion of 100% acetylated proteins, we used *E. coli* lysate as a model system (because SILAC mouse liver tissue is not arginine-labeled, we cannot quantify how acetylation affects these peptides). Peptides generated by cleavage at arginine residues (arginine-flanked, AF) were compared between 100% acetylated and control-treated samples. Hundred percent acetylation caused a slight reduction in the median ratio of AF peptides, indicating a slight decrease in AF peptide cleavage after 100% acetylation. In addition, the distribution of AF peptides after 100% acetylation was broader than in the control sample, indicating greater variability in peptide cleavage (which may contribute to inaccurate measurements using this method) (Appendix Fig S6). In order to ensure that our ratio measurements were accurate, we only considered measurements that were consistent between two dilutions; for example, the ratio at 0.01% stoichiometry should be 10× less than at 1% stoichiometry. Since ratio measurements are imprecise, we allowed a 2-fold deviation from the expected 10× difference (5× to 20×). This was an important control since many ratios did not show a linear relationship with the dilution series, indicating that these measurements were inaccurate.

Expanded View for this article is available online:
http://emboj.embopress.org

Acknowledgements
We thank the members of the department of proteomics at CPR for their helpful discussions, Patrick Matthias for providing murine embryonic fibroblasts, and Jeremy Daniels for providing mouse liver tissues. We thank the Matthias Mann laboratory, Felix Meissner, and Steven Dewitz for providing SILAC liver tissue; and Richard Scheltema for helpful discussion of the data. This work was supported by the Hallas Møller Investigator Fellowship to CC from the Novo Nordisk Foundation. The Center for Protein Research is funded by a generous grant from the Novo Nordisk Foundation (NNF14CC0001).

Author contributions
BTW and CC conceived the project and prepared the manuscript. BTW performed mass spectrometry analysis and analyzed the data. VI assisted with mass spectrometry and computational analysis of TMT reporter ions. TM and RZ provided tissues from fed, fasted, and ATGL-deficient mice. All authors critically reviewed the manuscript. CC directed and supervised all aspects of the study.

Conflict of interest
The authors declare that they have no conflict of interest.

References

Choudhary C, Kumar C, Gnad F, Nielsen ML, Rehman M, Walther TC, Olsen JV, Mann M (2009) Lysine acetylation targets protein complexes and co-regulates major cellular functions. *Science (New York, NY)* 325: 834 – 840

Cox J, Neuhauser N, Michalski A, Scheltema RA, Olsen JV, Mann M (2011) Andromeda: a peptide search engine integrated into the MaxQuant environment. *J Proteome Res* 10: 1794 – 1805

Du J, Zhou Y, Su X, Yu JJ, Khan S, Jiang H, Kim J, Woo J, Kim JH, Choi BH, He B, Chen W, Zhang S, Cerione RA, Auwerx J, Hao Q, Lin H (2011) Sirt5 is a NAD-dependent protein lysine demalonylase and desuccinylase. *Science (New York, NY)* 334: 806 – 809

Fan J, Shan C, Kang HB, Elf S, Xie J, Tucker M, Gu TL, Aguiar M, Lonning S, Chen H, Mohammadi M, Britton LM, Garcia BA, Aleckovic M, Kang Y, Kaluz S, Devi N, Van Meir EG, Hitosugi T, Seo JH *et al* (2014) Tyr phosphorylation of PDP1 toggles recruitment between ACAT1 and SIRT3 to regulate the pyruvate dehydrogenase complex. *Mol Cell* 53: 534 – 548

Gerber SA, Rush J, Stemman O, Kirschner MW, Gygi SP (2003) Absolute quantification of proteins and phosphoproteins from cell lysates by tandem MS. *Proc Natl Acad Sci USA* 100: 6940 – 6945

Ghanta S, Grossmann RE, Brenner C (2013) Mitochondrial protein acetylation as a cell-intrinsic, evolutionary driver of fat storage: chemical and metabolic logic of acetyl-lysine modifications. *Crit Rev Biochem Mol Biol* 48: 561 – 574

Haemmerle G, Lass A, Zimmermann R, Gorkiewicz G, Meyer C, Rozman J, Heldmaier G, Maier R, Theussl C, Eder S, Kratky D, Wagner EF, Klingenspor M, Hoefler G, Zechner R (2006) Defective lipolysis and altered energy metabolism in mice lacking adipose triglyceride lipase. *Science (New York, NY)* 312: 734 – 737

Hallows WC, Yu W, Smith BC, Devries MK, Ellinger JJ, Someya S, Shortreed MR, Prolla T, Markley JL, Smith LM, Zhao S, Guan KL, Denu JM (2011) Sirt3 promotes the urea cycle and fatty acid oxidation during dietary restriction. *Mol Cell* 41: 139 – 149

Hebert AS, Dittenhafer-Reed KE, Yu W, Bailey DJ, Selen ES, Boersma MD, Carson JJ, Tonelli M, Balloon AJ, Higbee AJ, Westphall MS, Pagliarini DJ, Prolla TA, Assadi-Porter F, Roy S, Denu JM, Coon JJ (2013) Calorie restriction and SIRT3 trigger global reprogramming of the mitochondrial protein acetylome. *Mol Cell* 49: 186 – 199

Hirschey MD, Shimazu T, Goetzman E, Jing E, Schwer B, Lombard DB, Grueter CA, Harris C, Biddinger S, Ilkayeva OR, Stevens RD, Li Y, Saha AK, Ruderman NB, Bain JR, Newgard CB, Farese RV Jr, Alt FW, Kahn CR, Verdin E (2010) SIRT3 regulates mitochondrial fatty-acid oxidation by reversible enzyme deacetylation. *Nature* 464: 121 – 125

Jing E, O'Neill BT, Rardin MJ, Kleinridders A, Ilkeyeva OR, Ussar S, Bain JR, Lee KY, Verdin EM, Newgard CB, Gibson BW, Kahn CR (2013) Sirt3 regulates metabolic flexibility of skeletal muscle through reversible enzymatic deacetylation. *Diabetes* 62: 3404 – 3417

Kelstrup CD, Young C, Lavallee R, Nielsen ML, Olsen JV (2012) Optimized fast and sensitive acquisition methods for shotgun proteomics on a quadrupole orbitrap mass spectrometer. *J Proteome Res* 11: 3487 – 3497

Kim SC, Sprung R, Chen Y, Xu Y, Ball H, Pei J, Cheng T, Kho Y, Xiao H, Xiao L, Grishin NV, White M, Yang XJ, Zhao Y (2006) Substrate and functional diversity of lysine acetylation revealed by a proteomics survey. *Mol Cell* 23: 607 – 618

Lin H, Su X, He B (2012) Protein lysine acylation and cysteine succination by intermediates of energy metabolism. *ACS Chem Biol* 7: 947 – 960

Lundby A, Lage K, Weinert BT, Bekker-Jensen DB, Secher A, Skovgaard T, Kelstrup CD, Dmytriyev A, Choudhary C, Lundby C, Olsen JV (2012) Proteomic analysis of lysine acetylation sites in rat tissues reveals organ specificity and subcellular patterns. *Cell Rep* 2: 419 – 431

Newman JC, He W, Verdin E (2012) Mitochondrial protein acylation and intermediary metabolism: regulation by sirtuins and implications for metabolic disease. *J Biol Chem* 287: 42436 – 42443

Olsen JV, Vermeulen M, Santamaria A, Kumar C, Miller ML, Jensen LJ, Gnad F, Cox J, Jensen TS, Nigg EA, Brunak S, Mann M (2010) Quantitative phosphoproteomics reveals widespread full phosphorylation site occupancy during mitosis. *Sci Signal* 3: ra3

Ong SE, Blagoev B, Kratchmarova I, Kristensen DB, Steen H, Pandey A, Mann M (2002) Stable isotope labeling by amino acids in cell culture, SILAC, as a simple and accurate approach to expression proteomics. *Mol Cell Proteomics* 1: 376 – 386

Palacios OM, Carmona JJ, Michan S, Chen KY, Manabe Y, Ward JL 3rd, Goodyear LJ, Tong Q (2009) Diet and exercise signals regulate SIRT3 and activate AMPK and PGC-1alpha in skeletal muscle. *Aging* 1: 771 – 783

Park J, Chen Y, Tishkoff DX, Peng C, Tan M, Dai L, Xie Z, Zhang Y, Zwaans BM, Skinner ME, Lombard DB, Zhao Y (2013) SIRT5-mediated lysine desuccinylation impacts diverse metabolic pathways. *Mol Cell* 50: 919 – 930

Pougovkina O, Te Brinke H, Ofman R, van Cruchten AG, Kulik W, Wanders RJ, Houten SM, de Boer VC (2014) Mitochondrial protein acetylation is driven by acetyl-CoA from fatty acid oxidation. *Hum Mol Genet* 23: 3513 – 3522

Qiu X, Brown K, Hirschey MD, Verdin E, Chen D (2010) Calorie restriction reduces oxidative stress by SIRT3-mediated SOD2 activation. *Cell Metab* 12: 662 – 667

Rardin MJ, He W, Nishida Y, Newman JC, Carrico C, Danielson SR, Guo A, Gut P, Sahu AK, Li B, Uppala R, Fitch M, Riiff T, Zhu L, Zhou J, Mulhern D, Stevens RD, Ilkayeva OR, Newgard CB, Jacobson MP *et al* (2013a) SIRT5 regulates the mitochondrial lysine succinylome and metabolic networks. *Cell Metab* 18: 920 – 933

Rardin MJ, Newman JC, Held JM, Cusack MP, Sorensen DJ, Li B, Schilling B, Mooney SD, Kahn CR, Verdin E, Gibson BW (2013b) Label-free quantitative proteomics of the lysine acetylome in mitochondria identifies substrates of SIRT3 in metabolic pathways. *Proc Natl Acad Sci USA* 110: 6601 – 6606

Rolef Ben-Shahar T, Heeger S, Lehane C, East P, Flynn H, Skehel M, Uhlmann F (2008) Eco1-dependent cohesin acetylation during establishment of sister chromatid cohesion. *Science (New York, NY)* 321: 563 – 566

Schwer B, Eckersdorff M, Li Y, Silva JC, Fermin D, Kurtev MV, Giallourakis C, Comb MJ, Alt FW, Lombard DB (2009) Calorie restriction alters mitochondrial protein acetylation. *Aging Cell* 8: 604 – 606

Scott I, Webster BR, Li JH, Sack MN (2012) Identification of a molecular component of the mitochondrial acetyltransferase programme: a novel role for GCN5L1. *Biochem J* 443: 655 – 661

Shahbazian MD, Grunstein M (2007) Functions of site-specific histone acetylation and deacetylation. *Annu Rev Biochem* 76: 75 – 100

Shi T, Wang F, Stieren E, Tong Q (2005) SIRT3, a mitochondrial sirtuin deacetylase, regulates mitochondrial function and thermogenesis in brown adipocytes. *J Biol Chem* 280: 13560 – 13567

Shimazu T, Hirschey MD, Hua L, Dittenhafer-Reed KE, Schwer B, Lombard DB, Li Y, Bunkenborg J, Alt FW, Denu JM, Jacobson MP, Verdin E (2010) SIRT3 deacetylates mitochondrial 3-hydroxy-3-methylglutaryl CoA synthase 2 and regulates ketone body production. *Cell Metab* 12: 654 – 661

Sol EM, Wagner SA, Weinert BT, Kumar A, Kim HS, Deng CX, Choudhary C (2012) Proteomic investigations of lysine acetylation identify diverse substrates of mitochondrial deacetylase sirt3. *PLoS ONE* 7: e50545

Someya S, Yu W, Hallows WC, Xu J, Vann JM, Leeuwenburgh C, Tanokura M, Denu JM, Prolla TA (2010) Sirt3 mediates reduction of oxidative damage and prevention of age-related hearing loss under caloric restriction. *Cell* 143: 802 – 812

Still AJ, Floyd BJ, Hebert AS, Bingman CA, Carson JJ, Gunderson DR, Dolan BK, Grimsrud PA, Dittenhafer-Reed KE, Stapleton DS, Keller MP, Westphall MS, Denu JM, Attie AD, Coon JJ, Pagliarini DJ (2013) Quantification of mitochondrial acetylation dynamics highlights prominent sites of metabolic regulation. *J Biol Chem* 288: 26209 – 26219

Tan M, Peng C, Anderson Kristin A, Chhoy P, Xie Z, Dai L, Park J, Chen Y, Huang H, Zhang Y, Ro J, Wagner Gregory R, Green Michelle F, Madsen Andreas S, Schmiesing J, Peterson Brett S, Xu G, Ilkayeva Olga R, Muehlbauer Michael J, Braulke T *et al* (2014) Lysine glutarylation is a protein posttranslational modification regulated by SIRT5. *Cell Metab* 19: 605 – 617

Tao R, Coleman MC, Pennington JD, Ozden O, Park SH, Jiang H, Kim HS, Flynn CR, Hill S, Hayes McDonald W, Olivier AK, Spitz DR, Gius D (2010) Sirt3-mediated deacetylation of evolutionarily conserved lysine 122 regulates MnSOD activity in response to stress. *Mol Cell* 40: 893 – 904

Thompson A, Schafer J, Kuhn K, Kienle S, Schwarz J, Schmidt G, Neumann T, Johnstone R, Mohammed AK, Hamon C (2003) Tandem mass tags: a novel quantification strategy for comparative analysis of complex protein mixtures by MS/MS. *Anal Chem* 75: 1895 – 1904

Ting L, Rad R, Gygi SP, Haas W (2011) MS3 eliminates ratio distortion in isobaric multiplexed quantitative proteomics. *Nat Methods* 8: 937 – 940

Vizcaino JA, Cote RG, Csordas A, Dianes JA, Fabregat A, Foster JM, Griss J, Alpi E, Birim M, Contell J, O'Kelly G, Schoenegger A, Ovelleiro D, Perez-Riverol Y, Reisinger F, Rios D, Wang R, Hermjakob H (2013) The PRoteomics IDEntifications (PRIDE) database and associated tools: status in 2013. *Nucleic Acids Res* 41: D1063 – D1069

Wagner GR, Hirschey MD (2014) Nonenzymatic protein acylation as a carbon stress regulated by sirtuin deacylases. *Mol Cell* 54: 5 – 16

Wagner GR, Payne RM (2013) Widespread and enzyme-independent N{epsilon}-acetylation and N{epsilon}-succinylation of proteins in the chemical conditions of the mitochondrial matrix. *J Biol Chem* 288: 29036 – 29045

Wang Q, Zhang Y, Yang C, Xiong H, Lin Y, Yao J, Li H, Xie L, Zhao W, Yao Y, Ning ZB, Zeng R, Xiong Y, Guan KL, Zhao S, Zhao GP (2010) Acetylation of metabolic enzymes coordinates carbon source utilization and metabolic flux. *Science (New York, NY)* 327: 1004 – 1007

Weinert BT, Iesmantavicius V, Moustafa T, Scholz C, Wagner SA, Magnes C, Zechner R, Choudhary C (2014) Acetylation dynamics and stoichiometry in *Saccharomyces cerevisiae*. *Mol Syst Biol* 10: 716

Weinert BT, Iesmantavicius V, Wagner SA, Scholz C, Gummesson B, Beli P, Nystrom T, Choudhary C (2013a) Acetyl-phosphate is a critical determinant of lysine acetylation in *E. coli*. *Mol Cell* 51: 265 – 272

Weinert BT, Scholz C, Wagner SA, Iesmantavicius V, Su D, Daniel JA, Choudhary C (2013b) Lysine succinylation is a frequently occurring modification in prokaryotes and eukaryotes and extensively overlaps with acetylation. *Cell Rep* 4: 842 – 851

Wellen KE, Hatzivassiliou G, Sachdeva UM, Bui TV, Cross JR, Thompson CB (2009) ATP-citrate lyase links cellular metabolism to histone acetylation. *Science (New York, NY)* 324: 1076 – 1080

Zhang J, Shi X, Li Y, Kim BJ, Jia J, Huang Z, Yang T, Fu X, Jung SY, Wang Y, Zhang P, Kim ST, Pan X, Qin J (2008) Acetylation of Smc3 by Eco1 is required for S phase sister chromatid cohesion in both human and yeast. *Mol Cell* 31: 143 – 151

Zhao S, Xu W, Jiang W, Yu W, Lin Y, Zhang T, Yao J, Zhou L, Zeng Y, Li H, Li Y, Shi J, An W, Hancock SM, He F, Qin L, Chin J, Yang P, Chen X, Lei Q *et al* (2010) Regulation of cellular metabolism by protein lysine acetylation. *Science (New York, NY)* 327: 1000 – 1004

Zimmermann R, Lass A, Haemmerle G, Zechner R (2009) Fate of fat: the role of adipose triglyceride lipase in lipolysis. *Biochim Biophys Acta* 1791: 494 – 500

